Waste Management 43 (2015) 176–187

Contents lists available at ScienceDirect

Waste Management

journal homepage: www.elsevier.com/locate/wasman

Coupling scales for modelling heavy metal vaporization from municipal solid waste incineration in a fluid bed by CFD

José Soria [a,*], Daniel Gauthier [b], Gilles Flamant [b], Rosa Rodriguez [c], Germán Mazza [a]

[a] Institute for Research and Development in Process Engineering, Biotechnology and Alternative Energies (PROBIEN, CONICET – UNCo), 1400 Buenos Aires St., 8300 Neuquén, Argentina
[b] Processes, Materials and Solar Energy Laboratory (PROMES-CNRS, UPR 8521), 7 Four Solaire Street, Odeillo, 66120 Font-Romeu, France
[c] Chemical Engineering Institute, National University of San Juan, 1109 Libertador (O) Avenue, 5400 San Juan, Argentina

ARTICLE INFO

Article history:
Received 8 January 2015
Accepted 14 May 2015
Available online 4 June 2015

Keywords:
Fluidized bed
Waste incineration
Heavy metal vaporization
Computational fluid dynamic
Two-scale model

ABSTRACT

Municipal Solid Waste Incineration (MSWI) in fluidized bed is a very interesting technology mainly due to high combustion efficiency, great flexibility for treating several types of waste fuels and reduction in pollutants emitted with the flue gas. However, there is a great concern with respect to the fate of heavy metals (HM) contained in MSW and their environmental impact. In this study, a coupled two-scale CFD model was developed for MSWI in a bubbling fluidized bed. It presents an original scheme that combines a single particle model and a global fluidized bed model in order to represent the HM vaporization during MSW combustion. Two of the most representative HM (Cd and Pb) with bed temperatures ranging between 923 and 1073 K have been considered. This new approach uses ANSYS FLUENT 14.0 as the modelling platform for the simulations along with a complete set of self-developed user-defined functions (UDFs). The simulation results are compared to the experimental data obtained previously by the research group in a lab-scale fluid bed incinerator. The comparison indicates that the proposed CFD model predicts well the evolution of the HM release for the bed temperatures analyzed. It shows that both bed temperature and bed dynamics have influence on the HM vaporization rate. It can be concluded that CFD is a rigorous tool that provides valuable information about HM vaporization and that the original two-scale simulation scheme adopted allows to better represent the actual particle behavior in a fluid bed incinerator.

1. Introduction

Worldwide, economic development along with rapidly population growth has resulted in a considerable increase in the generation of municipal solid waste (MSW). With the lack of space for new landfills and the environmental impact of MSW disposal, waste-to-energy processes are playing an increasingly important role in waste management (Cheng and Hu, 2010).

In this context, incineration represents an effective option for MSW treatment since it offers several advantages such as reducing waste volume, decreasing its reactivity and destroying biological threats, while releasing thermal energy. However, depending on the waste composition, MSW incineration generates pollutants that may be found in the ash and flue gases: CO, CO_2, NO_x, SO_x, VOCs, dioxins and furans, and heavy metals (HM). These issues have lead for the development of new "environmental friendly" techniques. In this sense, fluidized bed units appear as a "clean technology" for waste incineration (Koornneef et al., 2007).

Fluidized bed incinerators are employed because of their high mixing capacity, combustion efficiency (>0.9) and minimization of pollutants emissions such as NO_x and SO_x (Oka, 2003; Ravelli et al., 2008; Khan et al., 2009). Good burnout results in a high conversion of fuel to energy. Therefore, the effective burnout may contribute, to some degree, to improved energy efficiency. Additionally, high heat transfer between the bed and immersed tubes increases the energy recovery efficiency rather than recovering heat from the flue gas (Yokoyama et al., 2001). But a pre-treatment of the feedstock is needed, increasing the energy consumption, which results in a combined heat and power efficiency above 0.70, that is slightly higher than that of moving grate furnaces (IEA Bioenergy, 2009) and higher than the minimal energy efficiency of 0.65 as required by the European Directive 2008/98/EC (Quiroga et al., 2010). Another advantage of fluidized bed incinerators is the lower maintenance cost, due to the absence of moving parts and to the reduced damage to the refractory because of low thermal shock. Indeed, the bed material behaves as a thermal flywheel (Werther and Ogada, 1999). However, the mechanism of multiphase flows presents a high degree of complexity, which constitutes a main challenge for researchers and process engineers (Crowe, 1998).

* Corresponding author. Tel.: +54 299 4490302.
E-mail address: jose.soria@probien.gob.ar (J. Soria).

http://dx.doi.org/10.1016/j.wasman.2015.05.021
0956-053X/

Nomenclature

C_D	drag coefficient (dimensionless)
c_p	specific heat capacity (J/(kg K))
d_p	particle diameter (m)
d_{pore}	pore diameter (m)
D	diffusivity (m^2/s)
D_L	bed diameter (m)
$e\%$	relative percentage error
e_p	particle emissivity (dimensionless)
e_{ss}	restitution coefficient (dimensionless)
Ea	activation energy (J/kmol)
Ea'	non-intrinsic activation energy (J/kmol)
f	drag factor (dimensionless)
g	gravitational acceleration (m^2/s)
$g_{0,ss}$	radial distribution coefficient (dimensionless)
$\underline{I}$	radiation intensity (J/(m^2 s))
$\underline{\underline{I}}$	stress tensor (dimensionless)
k	thermal conductivity (W/(m K))
k_0	pre-exponential Arrhenius' factor
k'_0	Non-intrinsic pre-exponential factor
K	permeability (m^2)
K_{gs}	gas/solid momentum exchange coefficient (dimensionless)
L_0	initial particle length (m)
M_w	molecular weight (kg/kmol)
p	pressure (Pa)
q	metal concentration in waste (mg/kg)
q_0	initial metal concentration in waste (mg/kg)
q_f	final metal concentration in waste (mg/kg)
r_i	reaction rate of i specie (kg/(m^3 s))
$\hat{r}_i$	reaction rate of i specie (kmol/(m^3 s))
r_j	j-th homogeneous reaction rate (kg/(m^3 s))
R	universal gas constant
R_0	initial particle radius (m)
$R_{v,i}$	viscous component of drag force (N/kg)
$R_{p,i}$	pressure component of drag force (N/kg)
$R_{m,i}$	virtual mass component of drag force (N/kg)
Re	Reynolds number (dimensionless)
S_{rad}	radiative source term (J/(m^3 s))
t	time (s)
T	temperature (K)
T_b	mean bed temperature (K)
U	superficial velocity (m/s)
U_{mf}	gas superficial velocity at minimum fluidization (m/s)
X	solid component mass fraction (dimensionless)
Y_i	gas species mass fraction (dimensionless)

Greek letters

α_i	stoichiometric coefficients for municipal solid waste devolatilization
β_{abs}	absorption coefficient (m^{-1})
β_{sca}	scattering coefficient (m^{-1})
γ	stoichiometric coefficient for carbon combustion (dimensionless)
ΔH	reaction enthalpy (J/kg)
ε	porosity (dimensionless)
ε_g	gas volume fraction (dimensionless)
ε_s	solids volume fraction (dimensionless)
Θ_s	granular temperature (m^2/s^2)
μ	gas viscosity (Pa s)
ρ	density (kg/m^3)
σ	Stefan–Boltzmann constant (5.672×10^{-8} W/m^2 K^4)
τ	particle tortuosity (dimensionless)
$\underline{\underline{\tau}}_s$	stress tensor (Pa)
ϕ_{gs}	transfer rate of kinetic energy (kg/(s^3 m))

Subscripts

0	initial
b	bed
C	residual carbon
eff	effective
g	gas
HM	heavy metal
i	species
j	reaction
K	Knudsen
mf	minimum fluidization
p	particle
pore	pore
s	solid
w	wall

On the one hand, waste incineration is a multiphasic process and experimental essays are difficult and costly, and on the other hand CFD provides a lot of high quality information. Therefore this technique is a useful and powerful tool for studying, designing and scaling up fluidized beds (Singh et al., 2013).

Specifically, there is a great concern on metal emissions produced by incineration units due to their toxicity for human health and their impact on environment. Indeed, whatever the method, including any thermal method, metals are not destroyed; hence, depending on their physical chemical properties, they may be emitted with the exhaust gases (otherwise, they can be partially retained by bed materials such as sand and ash). It is thus essential to understand their behavior so as to achieve a strict control of their emission.

Several authors have studied, both experimentally (Abanades, 2001; Sun et al., 2004; Rio et al., 2007; H. Zhang et al., 2008; Y. Zhang et al., 2008; Yu et al., 2012, 2013) and theoretically – by thermodynamic modelling – (Zhou et al., 2002; Sørum et al., 2003; Ménard et al., 2006; Mazza et al., 2009, 2010;), the heavy metal release from different kinds of particles. The metal speciation can be predicted from the waste and the gas compositions, but the transient system evolution cannot be predicted by thermodynamics calculations (Falcoz et al., 2009; Asthana et al., 2010b). Thus, the HM evolution must be investigated by kinetic studies in burning conditions.

More recently, Soria et al. (2013a) formulated and validated a single particle model for predicting Cd vaporization rates of combusting MSW pellets. Then, the model was extended to the case of Pb (Soria et al., 2013b). The particle model is required in order to predict not only the combustion rate but also the intra-particle temperature gradients, which determines HM vaporization. Indeed, if the influence of the internal transport mechanisms and heat sources are ignored, the average particle temperature is underestimated (Gera et al., 2002), as well as the HM vaporization rate.

Nonetheless, the local approach dealt with an isolated particle, neglecting the influence of the environment in which it is immersed. Consequently, a fluid bed model must be formulated and coupled to the former approach in order to account for the interaction between the fluidized bed dynamics and the MSW particle.

In this sense, this paper extends our first study (Soria et al., 2013a) by including the interaction between the burning particle and the fluidized bed dynamics, representing rigorously the actual process. In this two-scale scheme, the fluid bed simulation allows

accessing the set of variables in the immediate particle surroundings through its trajectory so as to accurately define the conditions at the local scale and improve the representation of the heat and mass transfer phenomena that take place during the residence time of the MSW particle in the bubbling fluidized bed.

In particular, the aim of this study is to develop a two-scale model that contemplates the influence of the bed fluid dynamics on both the thermal conversion of MSW pellets and the vaporization of Cd and Pb for bed temperatures comprised in the range 923–1073 K, and to compare the simulation results with experimental data obtained in a lab-scale fluidized bed incinerator reported by Falcoz et al. (2009).

1.1. Previous experimental work: Falcoz et al. (2009) experiments

Falcoz et al. (2009) studied the kinetics of HM vaporization from so-called realistic artificial waste (RAW) pellets made from MSW, in a laboratory fluidized bed reactor. These synthetic pellets were made from a mixture of real MSW, sand, glue and metallic salt that was pressed into cylinders and dried. The pellet physical properties along with the ultimate analysis are shown in Table 1. The experimental setup (Fig. 1) involved a high temperature, electrically-heated fluidized bed reactor coupled to a customized inductively coupled plasma optical emission spectrometer (ICP-OES).

Experiments were carried out with solid samples impregnated with Cd (or Pb) at 923, 1013, 1043, and 1073 K. Once at thermal steady state, a given mass of reactive metal-spiked particles was injected into the bed composed of sand where the concentration of the HM vaporized in the exhaust gas was measured online by ICP-OES technique. The vaporization rate at the particle level was then determined from the experimental concentration profile in the fluid bed outlet gas, by using the inverse method – from the model formulated by Kunii and Levenspiel (1968) – previously developed and validated by Abanades et al. (2005).

2. CFD modelling approach

2.1. Particle scale model (Soria et al., 2013a)

In the mathematical treatment for the combustion of very small particles, such as pulverized coal particles, the Biot number (hL/k) is generally much less than one, which justifies the assumption of uniform temperature inside the particle (Lu and Baxter, 2011; Momeni, 2012). Nonetheless, this condition does not apply to the MSW particles incinerated in this work (with size of about 1 cm), so the hypothesis of uniform temperature distribution is no longer valid (Lu and Baxter, 2011), increasing the inherent complexity of the incineration process and its modelling. Additionally, the temperature gradients generated in the particle affect the HM

Table 1
Particle properties from Falcoz et al. (2009).

Property	ε_0	L_0 (m)	R_0 (m)	d_{pore} (μm)	$\rho_{app,0}$ (kg/m^3)	
Value	0.65	1.5×10^{-2}	0.5×10^{-2}	200	614	
Ultimate Analysis	C	H	O	N	S	Ash
Weight% (dry basis)	45.9	6.5	30.5	1.0	0.3	15.8
Proximate Analysis	Volatile matter		Fixed C		Ash + inerts	
Weight% (dry basis)	68.2		14.7		17.1	

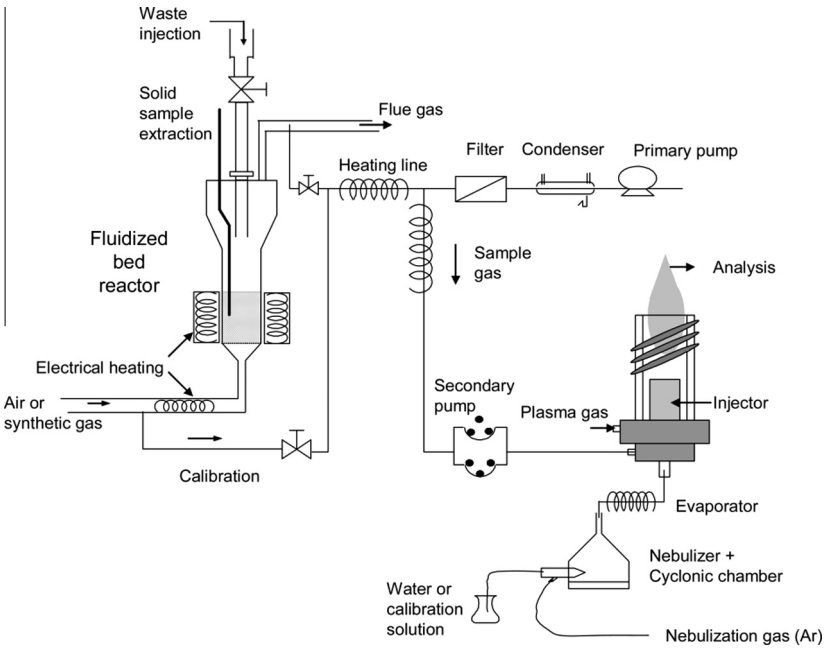

Fig. 1. Experimental set up from Falcoz et al. (2009). The fluidizing gas is preheated through a series of two electrical resistances. In order to measure the metal concentration in exhaust gases online, the nearby ICP (distance: 6 m) is connected to the gas outlet. The gas to be analyzed (sample gas) is carried to the ICP through a heated and insulated line (temperature: 250 °C). A second sampling line, by-passing the reactor, is used to obtain clean gas (i.e. metal free gas) for calibration protocol.

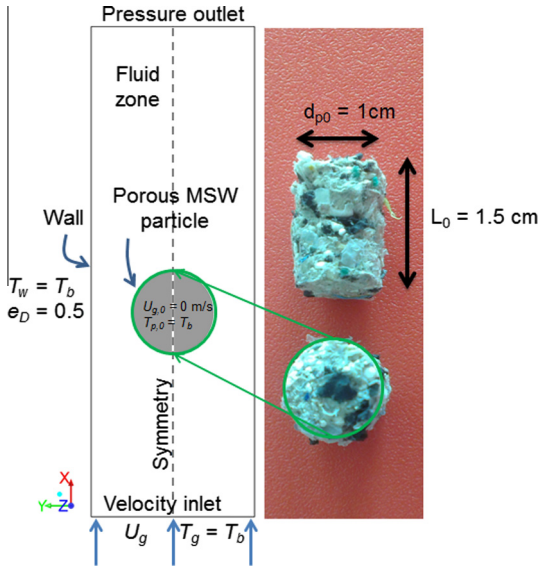

Fig. 2. Particle geometry and modelling configuration (Soria et al., 2013a). Figure shows the zoomed view of the adopted geometry along with the boundary conditions (the computational domain is larger than the particle). The porous waste particle is a cylinder of radius R_0 and height L_0. The direction of the inlet main flow – air – is perpendicular to the longitudinal axis of the particle. In order to avoid possible numerical complications, mainly gas backflow, the computational domain is set significantly larger.

vaporization rate, since it is very sensitive to the local temperature of the incinerated solid (Abanades et al., 2002; Sun et al., 2004). Thus, the intra-particle thermal gradient must be correctly predicted so as to accurately evaluate the HM vaporization rate. On this basis, the 2D CFD non-isothermal single particle model proposed by Soria et al. (2013a) is adopted for simulating the local phenomena. The main aspects, assumptions and formulations are briefly described next. The system geometry, along with boundary conditions, is depicted in Fig. 2.

2.1.1. Physical chemical stages

The model contemplates a simplified representation of the phenomena that take place during MSW incineration: devolatilization, homogeneous combustion and residual carbon (heterogeneous) combustion. A detailed description concerning thermal decomposition stages during the combustion of carbonaceous materials has been extensively reported in the literature (Basu, 2006; Lu et al., 2008; Puig-Arnavat et al., 2010; Soria et al., 2013). The stoichiometry and reaction rates for the processes involved are listed in Table 2.

Drying stage is not modelled since all the moisture content in the particle is previously removed in an oven, as part of the preparation procedure.

On the basis of the high heating rate in fluidized beds and that heating up and devolatilization time are significant lower than combustion time (Basu, 2006), it is assumed that the MSW pellet is heated to the bed temperature before char combustion starts. Hence, the heating up step is not modelled and devolatilization is treated as instantaneous with the coefficients reported by Ménard (2003) (Table 2). This assumption may deviate to some degree, but it is expected to include a kinetic devolatilization expression in future work. Additionally, the devolatilization enthalpy is assumed to be zero and the particle size is considered to remain constant through this stage (Soria et al., 2013a).

The heterogeneous combustion is modelled by an effective stoichiometry from the classical combustion reactions that produces a CO/CO_2 mixture, as can be seen in Eq. (32). The primary CO/CO_2 ratio is very significant for the calculation of the particle temperature during combustion (Manovic et al., 2008). Arthur's empirical expression is used to calculate the ratio CO/CO_2 (Ménard, 2003) and the intrinsic pre-exponential factor and the activation energy are taken from Cooper and Hallett (2000).

The high temperature and the oxidizing atmosphere existing in the bed environment produce the gasification reactions of the carbon residue to be negligible compared to the reaction with oxygen. Therefore, gasification stage is not included in the model formulation.

A simplified approach, which considers only the main reactions (Table 2), is used to deal with homogeneous combustion (Van Tiggelen, 1968; Dryer and Glassman, 1973; Howard et al., 1973). This assumption is based on the uncertainty in quantifying the devolatilization emissions and the slight importance of this step in the model (Mazza et al., 2009). Additionally, it is considered that these reactions may take place in the volume of the particle's pores as well as outside of it.

Table 2
Stoichiometry and reaction rates for the considered processes.

Devolatilization (instantaneous)

1 kg of pyrolyzable material $\rightarrow \alpha_{CO}$ kg of CO + α_{CO_2} kg of CO_2 + α_{H_2O} kg of H_2O + α_{CH_4} kg of CH_4 + α_{H_2} kg of H_2 + α_C kg of C

Species	CO	CO_2	H_2O	CH_4	H_2	C
α_i [mass of *i*/mass of pyrolyzable material]	0.378	0.133	0.111	0.178	0.022	0.177

Residual carbon combustion

$C + \gamma O_2 \rightarrow (2\gamma - 1)CO_2 + 2(1-\gamma)CO$ (1)

$\gamma = \frac{2+f_c}{2(1+f_c)}$; $f_c = \frac{C_{CO}}{C_{CO_2}} = 1340\exp(-\frac{63500}{RT})$ (2)

$r_C = k_{0,C}.T.e^{-\frac{Ea_C}{RT}}.C_{O_2}.S_v.(1-\varepsilon)$ (3)

Homogeneous reactions

$\hat{r}_j$	Reaction description	Reaction rate (kmol m^{-3} s^{-1})	k_0	*Ea* (J/kmol)	Ref.
1	$CO + \frac{1}{2}O_2 \rightarrow CO_2$	$k_{0,1}e^{-\frac{Ea_1}{RT}}C_{CO}C_{O_2}^{0.5}C_{H_2O}^{0.5}$	1.3×10^{11}	1.26×10^{08}	Howard et al. (1973)
2	$H_2 + \frac{1}{2}O_2 \rightarrow H_2O$	$k_{0,2}e^{-\frac{Ea_2}{RT}}C_{H_2}C_{O_2}$	1.1×10^{16}	7.50×10^{07}	Van Tiggelen (1968)
3	$CH_4 + \frac{3}{2}O_2 \rightarrow CO + 2H_2O$	$k_{0,3}e^{-\frac{Ea_3}{RT}}C_{CH_4}^{0.7}C_{O_2}^{0.8}$	5.01×10^{11}	2.01×10^{08}	Dryer and Glassman (1973)

HM vaporization

$HM_{MSW}(s) \rightarrow HM(g)$

$r_{HM} = k'_{0,HM}.e^{-\frac{Ea'_{HM}}{RT}}.\left(\frac{10^6 X_{HM} - q_f}{q_0 - q_f}\right)^n.10^{-6}.\rho_{app,o} + \frac{r_C.(10^6 X_{HM} - q_f)}{X_{C,0}}$ (4)

HM	q_0 (mg kg^{-1})	k_0' (mg kg^{-1} s^{-1})	Ea'/R (K)	*n*
Pb	754	2.92644×10^{18}	43,927	1.6
Cd	728	3.65119×10^{14}	32,926	1.4

Table 3
Governing equations.

Species mass transport equation	$\frac{\partial(\varepsilon\rho_g Y_i)}{\partial t} + \nabla\cdot(\rho_g U_g Y_i) = \nabla\cdot(D_{eff,i}\nabla Y_i) + r_i$	(5)
Overall gas-phase continuity equation	$\frac{\partial(\varepsilon\rho_g)}{\partial t} + \nabla\cdot(\rho_g U_g) = r_C$	(6)
Momentum equation for porous media	$\frac{\partial(\varepsilon\rho_g U_g)}{\partial t} + \nabla\cdot(\rho_g U_g U_g) = -\nabla p + \nabla\cdot(\tau) + B_f - \frac{\mu}{K}U_g$	(7)
Energy conservation equation	$(\rho c_p)_{pm}\frac{\partial T}{\partial t} + (\rho c_p)_f U_g \nabla T = \nabla\cdot(k_{eff}\nabla T) + \sum_{j=1}^{j=N} r_j.(-\Delta H_j) + r_C.(-\Delta H_C) + S_{rad}$	(8)
Radiative transfer equation	$\frac{dI(\vec{r},\vec{s})}{ds} + (\beta_{abs}+\beta_{sca})I(\vec{r},\vec{s}) = \beta_{abs}n^2\frac{\sigma T^4}{\pi} + \frac{\beta_{sca}}{4\pi}\int_0^{4\pi} I(\vec{r},\vec{s}')\phi(\vec{s},\vec{s}')d\Omega'$	(9)
Mass conservation equation for the residual carbon	$\rho_{app,0}\frac{dX_C}{dt} = -r_C$	(10)
Mass balances for HM in solid and gas phases	$\rho_{app,o}\frac{dX_{HM}}{dt} = -r_{HM}$	(11)
	$\frac{\partial(\varepsilon\rho_g Y_{HM})}{\partial t} + \nabla\cdot(\varepsilon\rho_g U_g Y_{HM}) = \nabla\cdot(D_{eff,HM}\nabla Y_{HM}) + r_{HM}$	(12)

During the consumption of the solid by combustion, HM is released and several transformations may occur to the HM (Asthana et al., 2010a).

The global process of HM vaporization from a combusting MSW particle can be represented as a hypothetical chemical reaction, that is:

$$HM_{MSW}(s) \rightarrow HM(g)$$

The subscript MSW indicates that this equation does not represent only HM vaporization but also the release as the result of the physical–chemical processes that take place during MSW incineration.

It is considered that HM release takes place as a result of vaporization and thermal degradation of the organic matrix in which it is trapped. Thus, the heavy metal vaporization rate is addressed by means of an effective expression (Eq. (35)), where two sources of HM release are considered. The first term relates the HM vaporization rate to the local temperature level by means of an Arrhenius-type equation (effective vaporization rate which comprises the processes of HM vaporization and of subsequent gas transport out of the waste particle), and the second one comprises the HM release rate by the waste thermal degradation (in this case, residual carbon combustion). The equation parameters and reaction order (non-intrinsic kinetic parameters) were obtained by a non-linear fit, and its values are given in Table 2. The data required to develop the effective HM rate equation are, for each operating bed temperature: (1) from the experiments: r_{HM}, $q_{0,HM}$, $q_{f,HM}$ and q; and (2) from CFD simulations: information that could not be provided experimentally such as average particle temperature and combustion rate (T_p and r_C). The simulations for obtaining the effective parameters are performed without considering HM vaporization but including all other physical chemical steps (instantaneous devolatilization, char combustion and devolatilization gas combustion) and mass and heat transport phenomena. This rate expression was established for fluidized bed temperatures ranging from 923 to 1073 K. Therefore it is limited to fluid beds and systems with similar conditions inducing high heating rates (several hundreds of degrees per second).

2.1.2. Governing equations, initial and boundary conditions

The species mass transport equation for each gas phase component ($i = N_2$, O_2, CO, CO_2, CH_4, H_2 and H_2O) along with the energy and mass conservations are given in Table 3, where r_i is the net production rate of species i by both homogeneous and heterogeneous chemical reactions in (kg/(m^3 s)), Y_i is the species mass fraction, ρ_g is the gas density and ε stands for the porosity.

The initial temperature of all system components (gas and particle) is considered to equalize the bulk bed temperature ($T_{g,0} = T_{p,0} = T_b$), where HM vaporization begins with the residual carbon combustion stage. The initial velocity inside the particle is set to zero so as to let gaseous species diffuse over time. The initial concentration inside the particle is the same as reported by Falcoz et al. (2009): $q_{0,Cd}$ = 728 mg/kg and $q_{0,Pb}$ = 754 mg/kg.

"Velocity inlet" boundary condition is used for the gas entering the control volume with a value given by the reactor scale model and the fluid bed mean temperature T_b. Additionally, species mass fraction for N_2 and O_2 were set as 0.77 and 0.23, respectively. Meanwhile the pressure is set at the limit of the geometry. Finally, the sidewall is considered to be representative of the bulk dense phase at T_b. Concerning the radiative heat transfer, a value of the isothermal radiant emissivity for the dense phase is estimated according to the expression reported by Mazza and Barreto (1994). Additionally, this wall is specified as a stationary wall with no slip and zero diffusive flux for all species. Finally, symmetry boundary condition is used to minimize the number of cell, reducing computational time.

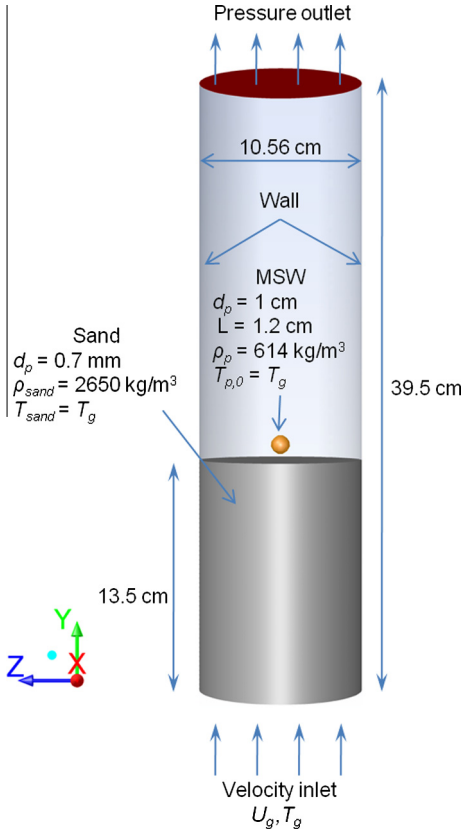

Fig. 3. Modelling configuration of the fluidized bed incinerator The lab-scale fluidized bed is modelled in CFD FLUENT software. It comprises a velocity inlet, wall and pressure outlet conditions. Initially, the MSW particle is placed at the bed surface. Hot air passes through the sand bed, producing the bed a fluidized state and the consequently particle dynamic behavior.

2.2. Fluidized bed model

The lab scale fluid bed incinerator employed by Falcoz et al. (2009) – installed in PROMES-CNRS laboratory and described in Section 1.1 – is modelled in 3D, with a cylindrical geometry representing the fluidized bed from the distributor to the top of the freeboard. The main geometric characteristics and operating conditions (in accordance with the settings of the experiment) are shown in Fig. 3.

In this system, air flows through the distribution plate, located at the base of the bed, with a superficial velocity U_g and temperature T_g equal to the bulk bed temperature. The bed is composed of silica sand with average particle diameter 700 μm (U_{mf} = 0.17 m/s), corresponding to Geldart B group.

The drag force exerted by the sand and the fluidizing agent (air) on the solid waste particle is calculated from the simulation onset. While in the bed, the particle can be surrounded by a bubble, by the emulsion phase, or it can even be in the freeboard. The model identifies the environment in which the particle is located and calculates the drag force based on a weighted average according to the local volume fraction of each phase.

The high mixing degree promoted by the bubbles allows the bed to absorb rapidly the local gradients generated by the few MSW combusting particles, thus maintaining the bed macroscopically isothermal. Additionally, the experimental temperature measurements reported by Falcoz (2008) showed, as expected, that due to the small amount of reactive particles injected into the bed, its mean temperature does not vary significantly, resulting in an increase always less than 20 K. Similar observations were reported by Abanades et al. (2003). Consequently, the simulations were performed considering that the bed operates isothermally from the macroscopic point of view, thus reducing computational time.

2.2.1. Multiphase flow governing equations, initial and boundary conditions

The momentum and mass conservation equations for a multiphase system were solved in order to simulate the bubbling fluidized bed fluid dynamics. The Eulerian approach was adopted to represent the mass and momentum transport for sand and the fluidizing air, while the kinetic theory for granular flow was used for the conservation of solid fluctuation energy.

The conservation equations along with the constitutive expressions are listed in Table 4.

Initially, the MSW particle is injected on the surface of the bed, so as to avoid the drastic change (and convergence problems associated with it) that the particle would suffer if it were injected once the fluid bed is vigorously fluidized.

Air velocity inlet was set at 0.54 m/s, that is 3 times greater than the minimum fluidizing velocity U_{mf}. Pressure outlet was selected for the top of the incinerator, with a value equal to the atmospheric pressure, while the incinerator wall was fixed as stationary wall without slip.

2.2.2. Macroscopic particle model (Agrawal et al., 2004)

The modelling of big (macroscopic) particles requires special treatment to take into account effects such as the blockage of fluid volume, the proper evolution of the drag force and torque experienced by the particles, particle–particle collisions as well as particle–wall collisions, and friction dynamics. In this work, the MSW pellet is treated with an original approach named "Macroscopic

Table 4
Fluid bed governing and constitutive equations.

Mass conservation		
	$\frac{\partial}{\partial t}(\varepsilon_g\rho_g)+\nabla.(\varepsilon_g\rho_g U_g)=0$	(13)
	$\frac{\partial}{\partial t}(\varepsilon_s\rho_s)+\nabla.(\varepsilon_s\rho_s U_s)=0$	(14)
Momentum conservation		
	$\frac{\partial}{\partial t}(\varepsilon_g\rho_g U_g)+\nabla\cdot(\varepsilon_g\rho_g U_g U_g)=-\varepsilon_g\nabla p+\nabla.\overline{\overline{\tau_g}}+\varepsilon_g\rho_g\vec{g}+\vec{R}_{gs}+S_m$	(15)
	$\frac{\partial}{\partial t}(\varepsilon_s\rho_s U_s)+\nabla\cdot(\varepsilon_s\rho_s U_s U_s)=-\varepsilon_s\nabla p-\nabla p_s+\nabla.\overline{\overline{\tau_s}}+\varepsilon_s\rho_s\vec{g}+\vec{R}_{gs}+S_m$	(16)
Solid-phase stress tensor		
	$\overline{\overline{\tau_s}}=\varepsilon_s\mu_s(\nabla U_s+\nabla U_s^T)+\varepsilon_s(\lambda_s-\frac{2}{3}\mu_s)\nabla\cdot U_s\overline{\overline{I_s}}$	(17)
Eqs. (15) and (16) are coupled by the force at the interphase $\vec{R}_{gs}$,		
	$\vec{R}_{gs}=K_{gs}(U_g-U_s)$	(18)
According to Gidaspow et al. (1992), the interphase exchange coefficient, K_{gs}, is given by		
When $\varepsilon_g>0.8$	$K_{gs}=\frac{3}{4}C_D\frac{\varepsilon_s\varepsilon_g\rho_g\lvert U_g-U_s\rvert}{d_s}\varepsilon_g^{-2.65}$	(19a)
When $\varepsilon_g\leqslant 0.8$	$K_{gs}=150\frac{\varepsilon_s^2\mu_g}{\varepsilon_g d_s^2}+1.75\frac{\varepsilon_s\rho_g\lvert U_g-U_s\rvert}{d_s}$	(19b)
Drag coefficient	$C_D=\frac{24}{\varepsilon_g Re_s}\left[1+0.15(\varepsilon_g Re_s)^{0.687}\right]$	(20)
Reynolds number	$Re_s=\frac{\rho_g d_s\lvert U_g-U_s\rvert}{\mu_g}$	(21)
Solid pressure	$p_s=\varepsilon_s\rho_s\Theta_s+2\rho_s(1+e_{ss})\varepsilon_s^2 g_{0,ss}\Theta_s$	(22)
Radial distribution function	$g_{0,ss}=\left[1-\left(\frac{\varepsilon_s}{\varepsilon_{s,max}}\right)^{1/3}\right]^{-1}$	(23)
Solids shear viscosity	$\mu_s=\mu_{s,col}+\mu_{s,kin}+\mu_{s,fr}$	(24)
Solids' collision viscosity	$\mu_{s,col}=\frac{4}{5}\varepsilon_s\rho_s d_s g_{0,ss}(1+e_{ss})\sqrt{\frac{\Theta_s}{\pi}}$	(25)
Kinetic viscosity	$\mu_{s,kin}=\frac{10\rho_s d_s\sqrt{\Theta_s\pi}}{96\varepsilon_s g_{0,ss}(1+e_{ss})}\left[1+\frac{4}{5}\varepsilon_s g_{0,ss}(1+e_{ss})\right]^2$	(26)
Frictional viscosity	$\mu_{s,fr}=\frac{p_s sin(\phi_{gs})}{2\sqrt{I_{2D}}}$	(27)
Bulk viscosity	$\lambda_s=\frac{4}{3}\varepsilon_s\rho_s d_s g_{0,ss}(1+e_{ss})\sqrt{\frac{\Theta_s}{\pi}}$	(28)
Granular temperature equation	$\frac{3}{2}\left[\frac{\partial}{\partial t}(\varepsilon_s\rho_s\Theta_s)+\nabla\cdot(\varepsilon_s\rho_s U_s\Theta_s)\right]=(-p_s\overline{\overline{I_s}}+\overline{\overline{\tau_s}}):\nabla U_s+\nabla\cdot(k_{\Theta_s}\nabla\Theta_s)-\gamma_{\Theta_s}$	(29)
Granular temperature diffusion coefficient	$k_{\Theta_s}=\frac{150\rho_s d_s\sqrt{\Theta_s\pi}}{384 g_{0,ss}(1+e_{ss})}\left[1+\frac{6}{5}\varepsilon_s g_{0,ss}(1+e_{ss})\right]^2+2\rho_s\varepsilon_s^2 d_s g_{0,ss}(1+e_{ss})\sqrt{\frac{\Theta_s}{\pi}}$	(30)
Collision dissipation energy	$\gamma_{\Theta_s}=\frac{12(1-e_{ss}^2)g_{0,ss}}{d_s\sqrt{\pi}}\rho_s\varepsilon_s^2\Theta_s^{3/2}$	(31)

Particle Model (MPM)", formulated and validated by Agrawal et al. (2004), which considers all the effects described above (Agrawal et al., 2009).

In the MPM approach, on the one hand, the particle (that spans several computational cells) is treated under a Lagrangian frame of reference. At every time step of the unsteady simulation, a solid body velocity that describes the particle motion is fixed in the fluid cells within the particle volume (through momentum source/sink terms) to effectively transfer momentum from particle to fluid cells. On the other hand, drag and lift forces, as well as torques, acting on the particle are evaluated based on local velocity, pressure field and shear stress distribution. Moreover, MPM is structured in such a way that it automatically access the appropriate phase domain for the proper calculation of drag force on the particle based on the multiphase model selected.

However, up to now, the MPM does not allow to include any mass and energy source terms in order to take into account the effects of heterogeneous reactions, thus requiring a local approach. Hence, only the fluid dynamic interaction between the bed and the MSW pellet is simulated at the reactor scale.

Particle force balance and boundary conditions

A general force over the single fuel particle is given by:

$$\frac{dU_p}{dt} = F_{body} + F_{surf} + F_{coll} \tag{32}$$

The right hand side contains the body forces per unit particle mass (e.g. gravity, buoyancy) acting on each particle, the surface forces (e.g. drag, lift), and the particle–particle or particle–wall collision forces. These forces are used to compute the new velocities and positions of the particles at the next time step.

The calculation of drag between particle and the bed considers three contributions: viscous, pressure and virtual mass forces (Agrawal et al., 2009; Wadnerkar et al., 2010). Viscous component of fluid force/torque is calculated based on the shear stress distribution around the particle:

$$R_{v,i} = \sum_{\substack{surface \\ cells}} \sum_{j} \left(\vec{\tau}_{ji} d^2 \left(- \frac{\vec{r} \cdot \vec{x}_j}{|\vec{r} \cdot \vec{x}_j|} \right) \right) \tag{33}$$

where τ_{ji} is shear stress in the i direction on a plane perpendicular to j direction and this is the force exerted by the fluid in the region of greater j coordinates on the fluid of lesser j coordinates.

The pressure component of fluid force/torque is calculated based on pressure distribution around the particle:

$$R_{p,i} = \sum_{\substack{surface \\ cells}} \left(P d^2 \frac{\vec{r}}{|\vec{r}|} \cdot \vec{x}_i \right) \tag{34}$$

P and d^2 are pressure and approximated area of particle surface in a fluid cell that is partially occupied by the particle. The vectors of r and x_i are a radius vector from the fluid cell center to particle center and a unit vector for the Cartesian coordinates.

Virtual mass component of fluid force/torque is calculated as the integral of the rate of change of momentum for all fluid cells within particle volume.

$$R_{m,i} = \left[\sum_{\substack{volume \\ cells}} m_f U_{f,i} - \sum_{\substack{volume \\ cells}} m_f U_{p,i} \right] \frac{1}{\Delta t} \tag{35}$$

The sum of all these three components will provide total fluid surface force and torque on the particle.

$$R_i = R_{m,i} + R_{v,i} + R_{p,i} \tag{36}$$

After the calculation of these forces, equal and opposite source terms are applied to fluid flow equations.

Appropriate boundary conditions need to be specified when simulating the trajectories of dispersed phase particles. In this study, hard sphere collision algorithm is implemented for particle–wall collisions. Collisions are assumed binary and quasi-instantaneous and particle contact occurs at a point. Three parameters are employed to account for momentum dissipation during collision: normal restitution coefficient, tangential restitution coefficient and friction coefficient. A constant value of 0.8 was set for both coefficient of restitution (all normal and tangential momentum retained).

A two-way coupling between the bed and the particle is adopted. Such coupling occurs through volume fraction, ε, and exchange source term, S_m. The momentum exchange from the particle to continuous phase is just the opposite of the momentum transfer rate due to drag, lift and virtual mass forces exerted by the continuous phase on the particle.

2.3. Scales coupling

Fig. 4 schemes the calculation sequence adopted for simulating the coupled system. Isothermal fluid bed simulation (with MPM) initiates, solving the mass and momentum conservation equations. Once the bubbling regime is achieved (after 4 s in the simulation), it is considered that the incineration process (comprising char combustion, gas devolatilization combustion and HM vaporization) begins. Thus, the influence of the start-up of the fluid bed incinerator on the particle model is avoided. Then, every second, the code calculates the particle position and the relative velocity between the particle and the fluidizing air by a specifically created UDF, which is sent to the particle model as a boundary condition.

Then the single particle model solves the governing equations and calculates all the physical chemical processes, the intra-particle thermal gradient and the HM vaporization rate based on a more realistic fluid dynamic approach. Additionally, every second, the particle volumetric diameter is calculated and sent to the reactor scale model for determining the new drag forces, particle position and relative velocity, closing the loop. This numerical sequence continues until the waste pellet is totally consumed or the HM is vaporized.

2.4. Numerical solution

2.4.1. Particle scale model

Modelling at particle scale is carried out by 2D simulation. However, the dimension in the Z-axis (Fig. 2) is set as the particle's length in order to account for its volume (ANSYS, 2011). User-Defined Functions (UDFs) are programmed in C++ language and coupled to the software in order to simulate the heterogeneous processes of solid combustion and heavy metal vaporization. In addition, UDFs mass sources for each gas species participating in the residual carbon combustion, as well as UDFs for energy source due to heterogeneous combustion, viscous resistance, particle porosity change, absorption coefficient, effective diffusivities are also programmed.

Additionally, second order discretization scheme was used for all scalars in order to obtain more accurate results. The appropriate under-relaxation factors were set to avoid possible instabilities in the solution, thus reaching convergence in a lower iteration number. The radiative transfer equation was solved using the discrete ordinates method (DOM). The pixelation and angular discretization required by DOM in the frame of FLUENT are both established at 2×2. Finally, simulations were carried out in transient state, with a 0.01 s step size and 40 iterations per time step.

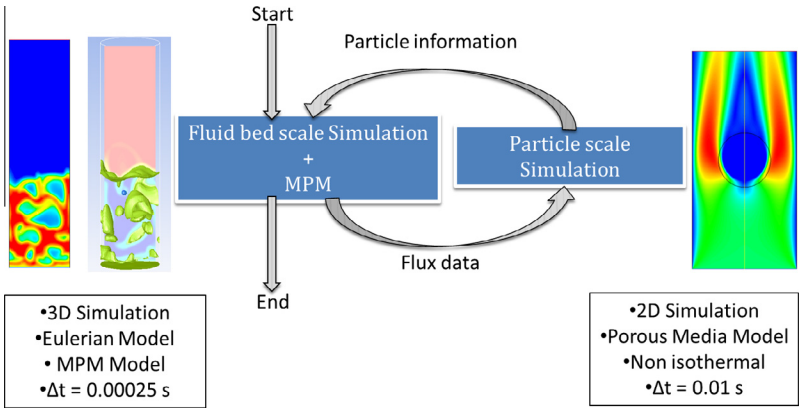

Fig. 4. Coupling scheme and information flux between fluid bed model and single particle model. It is represented the numerical sequence employed for solving the two-scale model. Fluid bed simulation (with MPM) initiates, solving the conservation equations and calculating the particle position and relative velocity between the particle and the fluidizing air by a specifically created UDF. Then, particle relative velocity information is sent to the particle model as boundary condition. Equations are solved in the single particle model for a time step and particle size is sent to the fluid bed model so as to calculate (and set) the drag factors in each direction.

Table 5
System properties and simulation parameters.

Property/parameter	Value	Commentary
Gas density (kg m^{-3})	$\rho_g = 0.3489$	Air ($T = 1013$ K)
Gas viscosity (kg m^{-1} s^{-1})	$\mu_g = 4.38 \times 10^{-5}$	Air ($T = 1013$ K)
Average particle diameter (mm)	0.7	Sand
Pellet density (kg m^{-3})	614	Measured
Restitution coefficient	0.9	Literature
Initial bed void fraction	0.48	Fixed bed
Superficial gas velocity (m s^{-1})	0.54	$3U_{mf}$
Initial bed height (m)	0.135	Fixed bed
Time step (s)	2.5×10^{-4}	Fixed
No. of iterations per time step	40	Fixed
Convergence criteria	10^{-6}	Fixed

2.4.2. Fluid bed scale model

Table 5 resumes air and sand properties along with the main parameters adopted, as well as initial conditions. It is a 3D simulation, with the mesh composed by 135,432 hexahedral cells, assuring the solid phase mass conservation in the whole fluidized bed. A self-developed UDF for obtaining the particle relative velocity was programmed and adjoined to the software calculus sequence.

For simulations at the bed scale, the cylindrical pellet used in the experiments is represented by a sphere with the same volume as that of the MSW particle, where the drag factor in each direction is calculated (as the actual length in the direction divided by the effective radius) and updated in the MPM, thus minimizing the shape difference impact on the drag and virtual mass forces.

All terms in the fluid bed model, except the unsteady formulation, were discretized using a second order scheme. The use of a small step time allows adopting a first order scheme for the unsteady formulation, achieving better stability with accuracy close to that of a second order scheme. The pressure and velocity are discretized by the Phase Coupled SIMPLE algorithm. Lastly, the unsteady simulation was performed with a 2.5×10^{-4} s step size and 40 iterations per time step.

3. Results and discussion

This section presents and analyzes the results obtained by simulating the coupled system: fluid bed hydrodynamics and particle model of a combusting pellet with heavy metal release.

3.1. Bed fluid dynamics

In order to validate the fluid bed dynamics, simulations for a sand/air fluidized bed were performed. As Falcoz et al. (2009) did not report pressure drop values, and with the aim of validating the drag model applied, CFD simulations of an experimental sand fluidized bed employed by Barreira Moreno (2007), geometrically similar to Falcoz's fluid bed, were performed and the results of pressure drop obtained were compared with the experimental data. It should be pointed out that both fluidized beds were meshed with the same type and size of elements. The operating conditions and geometric characteristics of the simulated fluidized bed are given in Table 6.

A good agreement is obtained between CFD results and experimental data (average relative error: 2.9%), confirming Gidaspow's drag model as an adequate expression for modelling the fluid dynamic behavior of the studied gas/sand fluidized bed.

Once the drag model was checked, CFD simulation regarding the MSW particle and the fluidized bed was carried out. Fig. 5 shows the fluidized bed behavior for different simulation times, indicating also the particle position. The particle moves in the bed promoted by different forces that transfer momentum to it. A bubbling regime is observed, with a typical flow pattern given by Geldart B particles where small bubbles are formed from the distributor and increase their sizes while rising through the bed as a result of coalescence, until they reach the bed's surface where they erupt, favouring the solids recirculation.

3.2. MSW particle motion

Among the different parameters that determine the discrete particle motion, the most important are the particle diameter and its density, since they influence the drag force, the virtual mass force, gravitational and buoyancy (Papadikis et al., 2009). The particle position (its trajectory during 1 s is shown in Fig. 6) results from the forces exerted by the gas and sand on the particle.

Table 6
Barreira Moreno (2007) experimental characteristics.

Superficial velocity range (m/s)	0.1–1
Bed diameter (m)	0.15
Fix bed height (m)	0.15
Particle diameter (sand) (mm)	0.7

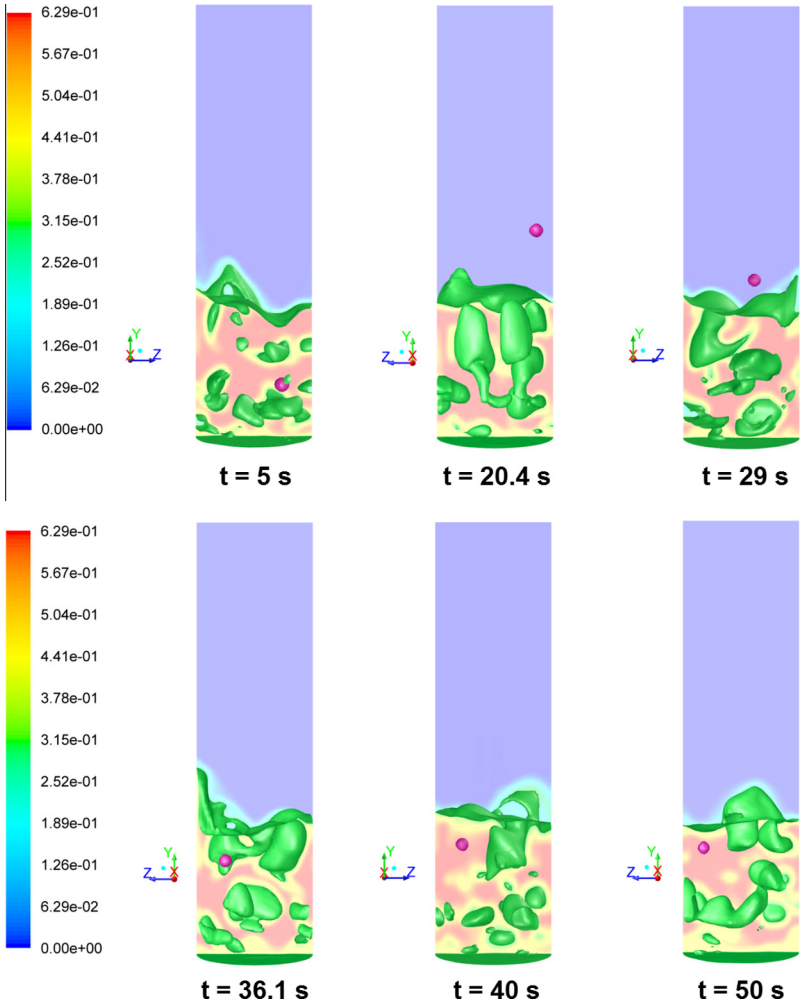

Fig. 5. Fluid bed dynamics and particle position. Figure describes the bubbling behavior, where a good mixing takes place and bubbles size increases as they rise in the bed.

These forces act in all three directions and depend on the particle size.

The bubble rising drags the particle up to the bed surface where bubbles erupt and the bed material is entrained toward the freeboard. However, the superficial gas velocity is less than the particle terminal velocity, so the latter is not carried out of the incinerator. Consequently, the particle returns to the bed surface, and eventually enters the bed. This penetration into the bed is mainly due to sand (which has also been driven by bubbles) that falls on the MSW particle, pushing and sinking it into the bed depth.

Additionally, CFD results show that the particle moves in the whole domain of the bed as a result of the high mixing degree promoted by the fluid bed, which agrees well with the observations reported by Abanades et al. (2003). The thermal analysis performed by these authors indicated that the combusting pellet travels in all bed regions, since a slight increase in the bed temperature (<20 K) was observed no matter the bed height, confirming CFD predictions.

3.3. Heavy metal vaporization

Figs. 7 and 8 illustrate the Cd and Pb vaporization rates for a MSW particle immerged in the incinerator, obtained with the coupled approach, and compare them against the experimental values reported, for all operating bed temperatures analyzed.

The temperature effect on the HM vaporization dynamics is well reproduced by the model: the higher the operating bed temperature, the higher the vaporization rate, resulting in a higher HM release (indicated by the area under the curve). Moreover, for the higher temperatures (1043 and 1073 K), there is a good agreement with the experimental results through the entire incineration process. However, for the lower temperatures (923 and 1013 K), the maximal vaporization rate predicted occurs before the maximal experimental rate. This discrepancy may be due to the assumption that the HM vaporization begins with the heterogeneous combustion stage that the HM release from the devolatilization step is disregarded. Nonetheless, the maximal rate values obtained from CFD simulations are very close to the experimental values, as shown in Table 7.

Figs. 7 and 8 also show how the bed fluid dynamics significantly influences the HM vaporization rate, especially at the beginning of the simulation. Since the relative particle velocity varies with time, the heterogeneous combustion rates oscillate during the process; thus provoking fluctuations in HM release rate, in contrast with the theoretical results reported by Soria et al. (2013a) where smooth vaporization curves were obtained as the result of adopting a constant value of relative particle velocity. However, as time elapses, the relative importance of this effect against the HM vaporization rate due to the particle thermal level diminishes gradually, and the simulation results follow the experimental data. Additionally, it can be appreciated that the influence of the bed

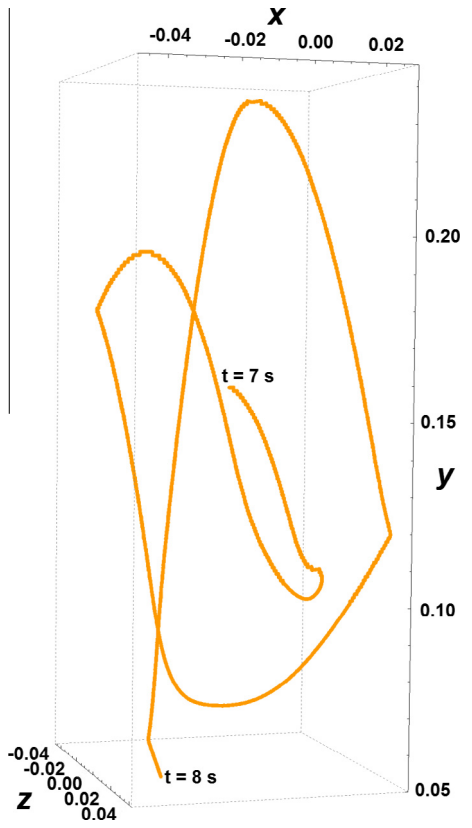

Fig. 6. MSW pellet trajectory (from t = 7 s to t = 8 s) It can be seen that the MSW particle moves in the whole domain of the bed, since the fluidizing velocity guarantees a similar behavior to that of the sand.

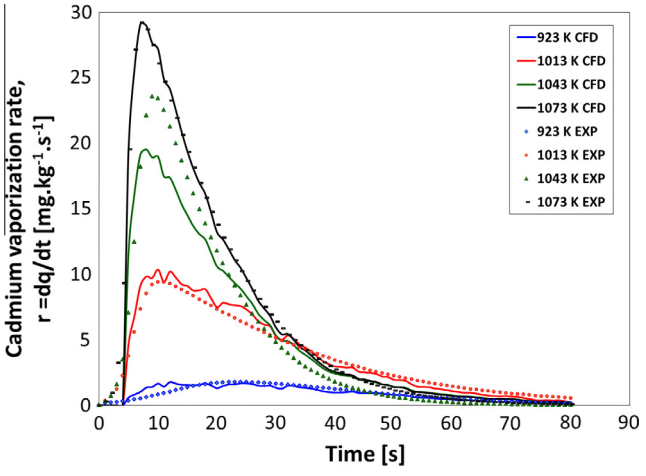

Fig. 7. Influence of temperature on the transient behavior of Cd vaporization rate. The higher the operative temperature, the higher the vaporization rate is. It can also be appreciated the influence of the bed dynamics.

dynamics decreases as T_b increases (the relative importance of heterogeneous combustion contribution on HM vaporization rate diminishes for higher bed temperature values), obtaining a very good agreement for the highest bed temperature analyzed (only a few oscillations initially).

Finally, Fig. 9 (Cd) and Fig. 10 (Pb) compare, for different bulk bed temperatures, the predicted temporal profiles of HM concentration in the burning waste particle with the experimental profiles. The comparison is very satisfactory, and results show how

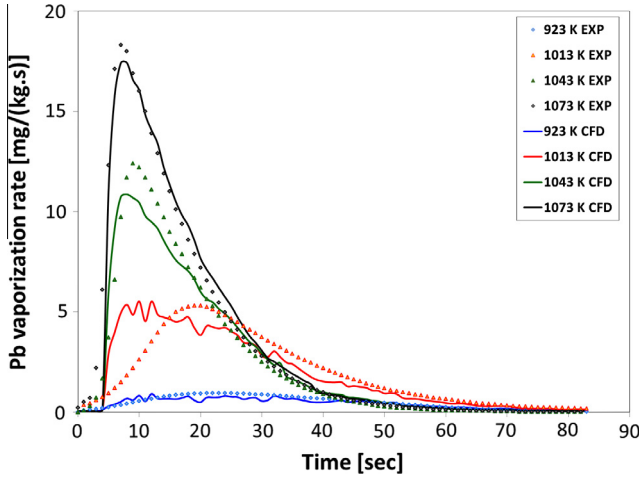

Fig. 8. Influence of temperature on the transient behavior of Pb vaporization rate. The higher the operative temperature, the higher the vaporization rate is. Nonetheless, Pb vaporization rate is lower than for the case of Cd. It can also be appreciated the influence of the bed dynamics.

Table 7
Comparison of maximal values of r_{HM}.

T (K)	$r_{HM,max}$ [EXP]	$r_{HM,max}$ [CFD]	e%
Cd			
923	1.780	1.782	−0.112
1013	9.439	10.365	−9.806
1043	23.580	19.541	17.130
1073	29.217	29.107	0.376
Pb			
923	0.942	0.909	3.470
1013	5.300	5.525	−4.254
1043	12.400	10.857	12.441
1073	18.300	17.412	4.851

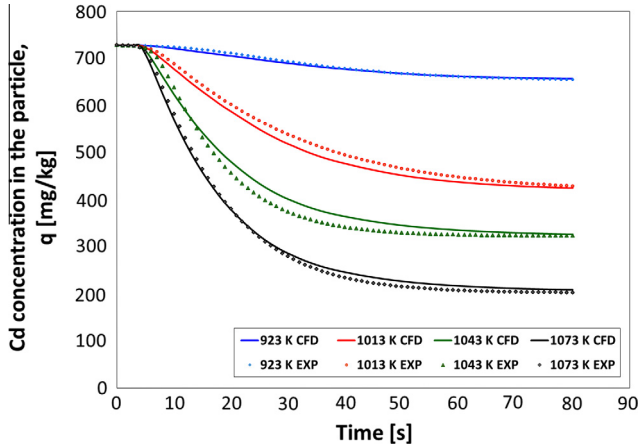

Fig. 9. Experimental and theoretical results of transient Cd concentration. The model prediction of Cd concentration evolution through time agrees well with the experimental data.

significantly temperature affects the metal vaporization: the higher the operating bed temperature T_b, the lower the HM residual quantity in the particle, q_f.

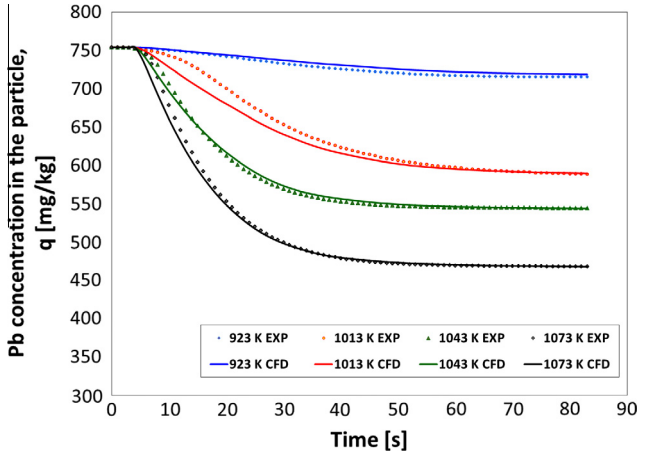

Fig. 10. Experimental and theoretical results of transient Pb concentration. The model prediction of Pb concentration evolution through time agrees well with the experimental data.

4. Conclusions

A CFD two-scale model was formulated to describe heavy metal vaporization from a combusting MSW particle in a bubbling fluidized bed. A CFD non-isothermal particle model, previously developed by the research group, was coupled to a fluid bed model in order to include the bed fluid dynamic effect on the HM (Cd and Pb) vaporization rate and achieve a more comprehensive study of the process.

With this new approach, the assumption of constant relative gas velocity used in the previous particle scale model (Soria et al., 2013a) is avoided, thus representing a considerable improvement and a better approximation of the real behavior of the studied phenomena.

CFD predictions fit satisfactorily the experimental data obtained in a laboratory scale fluid bed incinerator, thus validating this methodology as a useful tool for better understanding HM vaporization from burning fuel particle. Moreover, simulation results show that:

- The model predicts accurately the flow pattern under bubbling regime, with a typical bubble growth corresponding to Geldart B particles;
- the model represents well the MSW pellet – fluid bed interaction;
- the model takes into account the influence of bed dynamics on the combustion stage and the intra-particle heat transport mechanisms, which strongly impacts on the HM vaporization rate level.

On the basis of the reported results, the CFD model provides a rigorous description of the process along with useful information such as particle trajectories, residence time and char combustion rate, as well as thermal gradient inside large particles and heavy metal release. It is indeed the coupling of the fluid bed dynamics with the chemical phenomena, including toxic metal vaporization, occurring during the incineration of a MSW particle. Consequently, this two-scale approach should be helpful for accurately design and operate fluidized bed boilers under clean conditions.

Finally, future work includes the development of a kinetic devolatilization model in order to evaluate the evolution of volatile fraction, eliminating the assumption of instantaneous devolatilization.

Acknowledgements

This study was supported by the Argentinean–French ECOS SUD-MINCyT N° A11E01 collaboration agreement. G. Mazza is a Research Member of CONICET (Argentine). The first author is especially grateful to Scientific and Technical Research Council of Argentina (CONICET) for granting his Postdoctoral stage.

References

Abanades, S., 2001. Behavior of Heavy Metals During Municipal Solid Waste Incineration. PhD Thesis, University of Perpignan, France (in French).
Abanades, S., Flamant, G., Gauthier, D., 2002. Kinetics of heavy metal vaporization from model wastes in a fluidized bed. Environ. Sci. Technol. 36, 3879–3884.
Abanades, S., Flamant, G., Gauthier, D., 2003. The kinetics of vaporization of a heavy metal from a fluidized waste by an inverse method. Combust. Flame 134, 315–326. http://dx.doi.org/10.1016/S0010-2180(03)00097-X.
Abanades, S., Flamant, G., Gauthier, D., Tomas, S., Huang, L., 2005. Development of an inverse method to identify the kinetics of heavy metal release during waste incineration in fluidized bed. J. Hazard. Mater. 124, 19–26. http://dx.doi.org/10.1016/j.jhazmat.2005.05.004.
Agrawal, M., Bakker, A., Prinkey, M.T., 2004. Macroscopic particle model: tracking big particles in CFD. In: AIChE 2004 Annual Meeting.
Agrawal, M., Ookawara, S., Ogawa, K., 2009. Drag force formulation in macroscopic particle model and its validation. In: Proc. of 2009 AIChE. pp. 1–3.
ANSYS, 2011. ANSYS FLUENT Theory Guide.
Asthana, A., Falcoz, Q., Sessiecq, P., Patisson, F., 2010a. Modeling kinetics of Cd, Pb, and Zn vaporization during municipal solid waste bed incineration. Ind. Eng. Chem. Res. 49, 7605–7609. http://dx.doi.org/10.1021/ie100181x.
Asthana, A., Ménard, Y., Sessiecq, P., Patisson, F., 2010b. Modeling on-grate MSW incineration with experimental validation in a batch incinerator. Ind. Eng. Chem. Res. 49, 7597–7604.
Barreira Moreno, V.M., 2007. Hydrodynamic Study of a Fluidized Bed. Grade Thesis. University Carlos III of Madrid (in Spanish).
Basu, P., 2006. Combustion and Gasification in Fluidized Beds. Taylor and Francis Group LLC.
Cheng, H., Hu, Y., 2010. Municipal solid waste (MSW) as a renewable source of energy: current and future practices in China. Bioresour. Technol. 101, 3816–3824. http://dx.doi.org/10.1016/j.biortech.2010.01.040.
Cooper, J., Hallett, W.L.H., 2000. A numerical model for packed-bed combustion of char particles. Chem. Eng. Sci. 55, 4451–4460. http://dx.doi.org/10.1016/S0009-2509(00)00097-X.
Crowe, C.T., 1998. Multiphase Flows with Droplets and Particles. CRC Press, Boca Raton.
Dryer, F., Glassman, I., 1973. High-temperature oxidation of CO and CH_4. Symp. Combust. 14, 987–1003.
Falcoz, Q., 2008. Heavy Metal Vaporization During Municipal Waste Incineration: Kinetics and Transfer Processes. Ph.D. Thesis, Université de Perpignan, France (in French).
Falcoz, Q., Gauthier, D., Abanades, S., Flamant, G., Patisson, F., 2009. Kinetic rate laws of Cd, Pb, and Zn vaporization during municipal solid waste incineration. Environ. Sci. Technol. 43, 2184–2189.
Gera, D., Mathur, M.P., Freeman, M.C., Robinson, A., 2002. Effect of large aspect ratio of biomass particles on carbon burnout in a utility boiler. Energy Fuels 16, 1523–1532. http://dx.doi.org/10.1021/ef0200931.
Gidaspow, D., Bezburuah, R., Ding, J., 1992. Hydrodynamics of circulating fluidized beds: Kinetic theory approach. In: Fluidization VII: Proceedings of the 7th Engineering Foundation Conference on Fluidization. pp. 75–82.
Howard, J.B., Williams, G.C., Fine, D.H., 1973. Kinetics of carbon monoxide oxidation in postflame gases. Symp. Combust. 14, 975–986.
IEA Bioenergy, 2009. Accomplishments from IEA Bioenergy Task 36: Integrating Energy Recovery into Solid Waste Management Systems (2007–2009). End of Tasks Report, International Energy Agency (IEA).
Khan, A.A., de Jong, W., Jansens, P.J., Spliethoff, H., 2009. Biomass combustion in fluidized bed boilers: potential problems and remedies. Fuel Process. Technol. 90, 21–50. http://dx.doi.org/10.1016/j.fuproc.2008.07.012.
Koornneef, J., Junginger, M., Faaij, A., 2007. Development of fluidized bed combustion – an overview of trends, performance and cost. Prog. Energy Combust. Sci. 33, 19–55. http://dx.doi.org/10.1016/j.pecs.2006.07.001.
Kunii, D., Levenspiel, O., 1968. Bubbling bed model. Model for flow of gas through a fluidized bed. Ind. Eng. Chem. Fundam. 7, 446–452.
Lu, H., Baxter, L.L., 2011. Biomass combustion characteristics and implications for renewable energy. In: Grammelis, P. (Ed.), Solids Biofuels for Energy. Springer-Verlag, New York, pp. 95–121. http://dx.doi.org/10.1007/978-1-84996-393-0_5.
Lu, H., Robert, W., Peirce, G., Ripa, B., Baxter, L.L., 2008. Comprehensive study of biomass particle combustion. Energy Fuels 22, 2826–2839. http://dx.doi.org/10.1021/ef800006z.
Manovic, V., Komatina, M., Oka, S., 2008. Modeling the temperature in coal char particle during fluidized bed combustion. Fuel 87, 905–914. http://dx.doi.org/10.1016/j.fuel.2007.05.020.
Mazza, G., Barreto, G., 1994. Radiative heat transfer rates between gas-fluidized beds and immersed surfaces. Chem. Eng. Res. Des. 72, 441–454.

Mazza, G., Falcoz, Q., Gauthier, D., Flamant, G., 2009. A particulate model of solid waste incineration in a fluidized bed combining combustion and heavy metal vaporization. Combust. Flame 156, 2084–2092. http://dx.doi.org/10.1016/j.combustflame.2009.04.003.

Mazza, G., Falcoz, Q., Soria, J., Gauthier, D., Flamant, G., 2010. Nonisothermal particle modeling of municipal solid waste combustion with heavy metal vaporization. Combust. Flame 157, 2306–2317. http://dx.doi.org/10.1016/j.combustflame.2010.07.005.

Ménard, Y., 2003. Mathematical Modelling of Municipal Solid Waste Incineration and Thermodynamic Study of the Behaviour of Heavy Metals. Ph.D Thesis, Polytechnical National Institute of Lorraine, France (in French).

Ménard, Y., Asthana, a., Patisson, F., Sessiecq, P., Ablitzer, D., 2006. Thermodynamic study of heavy metals behaviour during municipal waste incineration. Process Saf. Environ. Prot. 84, 290–296. http://dx.doi.org/10.1205/psep.05166.

Momeni, M., 2012. Fundamental Study of Single Biomass Particle Combustion. Ph.D Thesis, University of Aalborg.

Oka, S., 2003. Fluidized Bed Combustion. In: Dekker, M., (Ed.). New York.

Papadikis, K., Gu, S., Bridgwater, A.V., 2009. CFD modelling of the fast pyrolysis of biomass in fluidised bed reactors: modelling the impact of biomass shrinkage. Chem. Eng. J. 149, 417–427. http://dx.doi.org/10.1016/j.cej.2009.01.036.

Puig-Arnavat, M., Bruno, J.C., Coronas, A., 2010. Review and analysis of biomass gasification models. Renew. Sustain. Energy Rev. 14, 2841–2851. http://dx.doi.org/10.1016/j.rser.2010.07.030.

Quiroga, G., Castrillón, L., Fernández-Nava, Y., Marañón, E., 2010. Physico-chemical analysis and calorific values of poultry manure. Waste Manage. 30, 880–884. http://dx.doi.org/10.1016/j.wasman.2009.12.016.

Ravelli, S., Perdichizzi, A., Barigozzi, G., 2008. Description, applications and numerical modelling of bubbling fluidized bed combustion in waste-to-energy plants. Prog. Energy Combust. Sci. 34, 224–253. http://dx.doi.org/10.1016/j.pecs.2007.07.002.

Rio, S., Verwilghen, C., Ramaroson, J., Nzihou, A., Sharrock, P., 2007. Heavy metal vaporization and abatement during thermal treatment of modified wastes. J. Hazard. Mater. 148, 521–528. http://dx.doi.org/10.1016/j.jhazmat.2007.03.009.

Singh, R.I., Brink, A., Hupa, M., 2013. CFD modeling to study fluidized bed combustion and gasification. Appl. Therm. Eng. 52, 585–614. http://dx.doi.org/10.1016/j.applthermaleng.2012.12.017.

Soria, J., Gauthier, D., Falcoz, Q., Flamant, G., Mazza, G., 2013a. Local CFD kinetic model of cadmium vaporization during fluid bed incineration of municipal solid waste. J. Hazard. Mater. 248–249, 276–284. http://dx.doi.org/10.1016/j.jhazmat.2013.01.015.

Soria, J., Reyes, A., Gauthier, D., Flamant, G., Mazza, G., 2013b. CFD kinetic rate law of Pb vaporization from waste pellets during fluidized bed combustion. Réc. Prog. Génie Procédés 104, 1–9.

Sørum, L., Frandsen, F.J., Hustad, J.E., 2003. On the fate of heavy metals in municipal solid waste combustion Part I: devolatilisation of heavy metals on the grate. Fuel 82, 2273–2283. http://dx.doi.org/10.1016/S0016-2361(03)00178-9.

Sun, L., Abanades, S., Lu, J., Flamant, G., Gauthier, D., 2004. Volatilization of heavy metals during incineration of municipal solid wastes. J. Environ. Sci. 16, 635–639.

Van Tiggelen, A., 1968. Oxidations et Combustions. Eds. Technip.

Wadnerkar, D., Agrawal, M., Pareek, V., 2010. Terminal velocity of particles falling in a non-newtonian yield pseudo-plastic fluids using a Macroscopic Particle model. In: 7th International Conference on Multiphase FLow. pp. 1–8.

Werther, J., Ogada, T., 1999. Sewage sludge combustion. Prog. Energy Combust. Sci. 25, 55–116.

Yokoyama, T., Suzuki, Y., Akiyama, H., 2001. Improvements and recent technology for fluidized bed waste incinerators. NKK Tech. Rev. 85, 38–43.

Yu, J., Sun, L., Xiang, J., Hu, S., Su, S., Qiu, J., 2012. Vaporization of heavy metals during thermal treatment of model solid waste in a fluidized bed incinerator. Chemosphere 86, 1122–1126. http://dx.doi.org/10.1016/j.chemosphere.2011.12.010.

Yu, J., Sun, L., Xiang, J., Hu, S., Su, S., 2013. Kinetic vaporization of heavy metals during fluidized bed thermal treatment of municipal solid waste. Waste Manage. 33, 340–346. http://dx.doi.org/10.1016/j.wasman.2012.11.006.

Zhang, H., He, P.-J., Shao, L.-M., 2008. Fate of heavy metals during municipal solid waste incineration in Shanghai. J. Hazard. Mater. 156, 365–373. http://dx.doi.org/10.1016/j.jhazmat.2007.12.025.

Zhang, Y., Chen, Y., Meng, A., Li, Q., Cheng, H., 2008. Experimental and thermodynamic investigation on transfer of cadmium influenced by sulfur and chlorine during municipal solid waste (MSW) incineration. J. Hazard. Mater. 153, 309–319. http://dx.doi.org/10.1016/j.jhazmat.2007.08.054.

Zhou, H., Abanades, S., Flamant, G., Gauthier, D., Lu, J., 2002. Simulation of heavy metal vaporization dynamics in a fluidized bed. Chem. Eng. Sci. 57, 2603–2614. http://dx.doi.org/10.1016/S0009-2509(02)00139-2.